ELSEVIER

Journal of Nuclear Materials 313–316 (2003) 1150–1155

journal of nuclear materials

www.elsevier.com/locate/jnucmat

Accumulation of impurities in advanced scenarios

R. Dux [a,*], C. Giroud [b], R. Neu [a], A.G. Peeters [a], J. Stober [a], K.-D. Zastrow [c], Contributors to the EFDA-JET Workprogramme, ASDEX Upgrade Team

[a] *Max-Planck-Institut für Plasmaphysik, EURATOM Association, Boltzmannstrasse 2-12, D-85748 Garching, Germany*
[b] *FOM-Ri jnhuizen, Ass. EURATOM-FOM, TEC, P.O. Box 1207, 3430 BE Nieuwegein, Netherlands*
[c] *EURATOM-UKAEA Fusion Association, Culham Science Centre, Abingdon OX14 3DB, UK*

Received 27 May 2002; accepted 26 September 2002

Abstract

Impurity behaviour in advanced scenarios at ASDEX Upgrade and JET has been investigated. For ASDEX Upgrade improved H-mode plasmas at $\delta = 0.35$, accumulation of tungsten and metallic impurities was observed inside $r/a = 0.3$ in cases with weak central heating. Central ECRH suppressed the accumulation by increasing the anomalous diffusion and by flattening the profile of the main plasma density which reduces neoclassical inward convection for the impurities. These effects are well described by impurity transport simulation and calculated v/D values agree with the measurements within a factor of 2. In JET reversed shear discharges with internal transport barriers, metallic impurities accumulate in cases with too strong peaking of the density profile. The peaking increases with the impurity charge and is low for the low-Z elements C and Ne as expected from neoclassical convection.

PACS: 52.25.Fi; 52.25.Vy; 52.55.Fa
Keywords: Impurity transport; Advanced scenarios; Impurity accumulation; Neoclassical transport

Impurity accumulation occurs when the radial density profile of an impurity evolves a stronger peaking than the profile of the main plasma ion. This is usually observed in the central part of the plasma inside a normalized radius $r/a < 0.5$. The high impurity concentration on axis leaves the main plasma impurity content and the total radiation loss nearly unchanged due to the small affected volume and vice versa the same impurity production at the vessel walls might produce largely different central impurity concentrations. The impurity sources are located in the edge region of the plasma and the equilibrium radial gradient of the impurity density n_i at radius r depends only on the ratio of the radial drift velocity v and the diffusion coefficient D at this radius.

$$\frac{1}{n_i}\frac{dn_i}{dr} = \frac{v}{D}. \tag{1}$$

The diffusion coefficient has an anomalous and a neoclassical contribution $D = D_{an} + D_{neo}$ and the convective transport, which is a necessary condition for impurity accumulation, is assumed to be purely neoclassical with $v = v_{neo}$. In a simplified treatment, only collisions of impurity and main ion D are considered and v_{neo} is for equal temperatures of both ion species $T_D = T_i$.

$$v_{neo} = D_{neo}\frac{Z_i}{Z_D}\left(\frac{1}{n_D}\frac{dn_D}{dr} - H\frac{1}{T_D}\frac{dT_D}{dr}\right). \tag{2}$$

The density gradient term drives an inwardly directed convective flux, while the temperature gradient yields an

* Corresponding author. Tel.: +49-89 3299 1256; fax: +49-89 3299 1812.
E-mail address: ralph.dux@ipp.mpg.de (R. Dux).

0022-3115/03/$ - see front matter
PII: S0022-3115(02)01508-8

outwardly directed drift velocity, where the factor H is always positive and has typical values $H = 0.2$–0.5. Thus, the normalized impurity density gradient is

$$\frac{1}{n_i}\frac{dn_i}{dr} = \frac{1}{n_D}\frac{dn_D}{dr}\frac{Z_i}{Z_D}\frac{D_{neo}}{D_{neo}+D_{an}}(1 - H\eta_D), \quad (3)$$

where η_D denotes the ratio of the normalized temperature gradient to the normalized main ion gradient. Eq. (3) shows, that impurity accumulation can only occur, if D_{an} is not too large compared to D_{neo} for plasmas with peaked ion density gradient at small η_D. In such a situation elements with higher charge number Z will accumulate stronger than low-Z elements. $D_{an} < D_{neo}$ is often observed in the central part of the plasma [1], however, sawtooth crashes periodically cause a flattening of the impurity profile. Advanced scenarios or plasmas with internal transport barrier (ITB) are thus of special concern with respect to impurity accumulation, since possible neoclassical inward convection is not suppressed by the low anomalous diffusive transport or by the sawtooth instability. In the following, impurity behaviour for advanced H-mode discharges in ASDEX Upgrade and for ITB plasmas with reversed shear in JET will be described.

1. Improved H-mode discharges at ASDEX Upgrade

In ASDEX Upgrade, almost all tiles of the central column are covered with tungsten [2], which due to its high-Z is very critical with respect to neoclassical transport. The investigated advanced scenarios are improved H-modes, which are characterized by a loss of the sawtooth activity and generally improved confinement over ordinary H-modes. Tungsten behaviour in other discharge scenarios can be found in [2]. Improved H-modes can be performed in quasi-steady state [3] and the operational space has recently been enlarged towards higher densities by increasing the triangularity of the plasma shape to $\delta = 0.35$ [4]. As in ordinary H-mode discharges at $\delta \approx 0.35$ without central heating, the density was observed to peak slowly throughout the discharge and a very strong peaking of the radiation power inside a poloidal flux label of $\rho \approx 0.3$ occurred, which can only be explained by accumulation of tungsten and other metallic impurities. In ordinary H-modes, addition of central ICRH or ECRH had shown to avoid impurity accumulation and the same recipe was applied in the improved H-mode scenario.

The effect of central ECRH on the impurity behaviour is demonstrated in Fig. 1. Various time traces of the improved H-mode discharge #15524 with $I_p = 1$ MA, $B_T = 2.5$ T, $\delta = 0.35$ and constant NBI heating power $P_{NI} = 5$ MW are shown. Central ECRH is applied from $t = 2.5$–4.5 s with $P_{ECRH} = 1.2$ MW from 2.5 to 3 s and

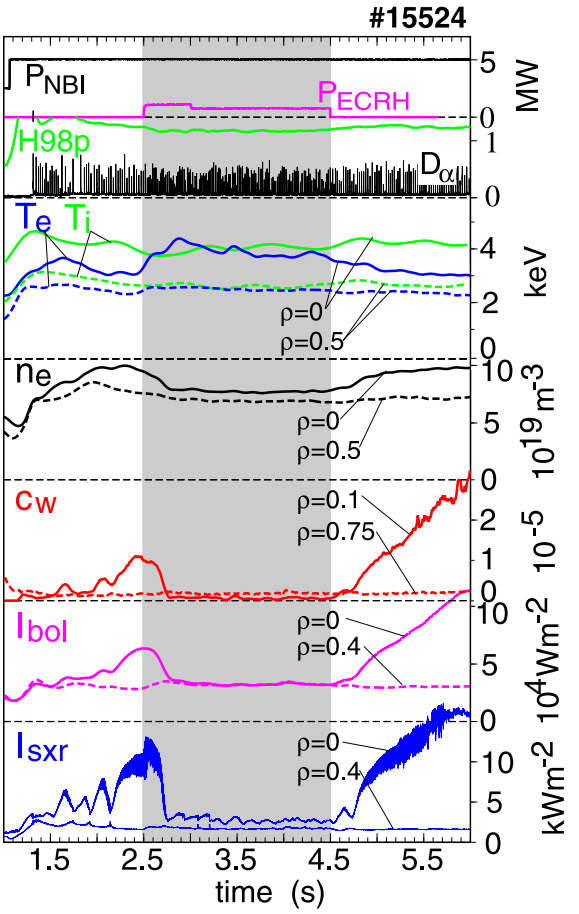

Fig. 1. Time traces for the improved H-mode discharge #15524 at ASDEX Upgrade.

$P_{ECRH} = 0.8$ MW from 3 to 4.5 s. During the ECRH phase, the thermal confinement time τ_E is reduced by ≈17% with respect to the pure NBI phase, while the scaled thermal confinement is only slightly reduced with $\tau_E/\tau_{ITERH-98p(y,th,2)} \approx 1.2$. The frequency of the type-I ELMs changes from $f_{ELM} = 50$ Hz to $f_{ELM} = 70$ Hz. n_e, T_e and T_i is depicted for $\rho = 0$ and $\rho = 0.5$. Only the central values are influenced with an increase of central T_e and a decrease of central n_e. A much stronger effect is found on the tungsten concentrations c_W, which are derived from spectroscopic measurements. c_W at $\rho = 0.75$ is deducted from the W quasi-continuum, which is emitted from ions around W^{28+} [5] and c_W at $\rho = 0.1$ from a Ni-like (W^{46+}) line at $\lambda = 0.793$ nm [6]. Accumulation of tungsten is suppressed by ECRH, i.e. the central W-concentration is reduced to the constant edge value of $c_W \approx 10^{-6}$. After the ECRH phase, c_W at $\rho = 0.1$ is steadily increasing and reaches $\approx 3 \times 10^{-5}$ at $t = 6$ s, which is 30 times the edge value. Total and soft X-ray radiation also evolve a strong peaking in the phases without ECRH. The total central emission is

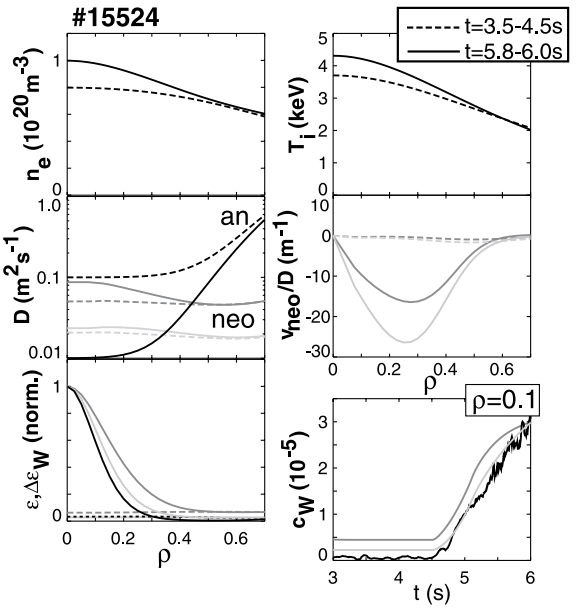

Fig. 2. Measured profiles of n_e, T_i, neoclassical transport coefficients of tungsten with (dark grey) and without (light grey) inclusion of additional impurities, used D_{an}, calculated tungsten radiation and measured total radiation for two time slices of #15524. In the lower right corner, a time traces of measured and simulated central tungsten concentration are shown.

approximately a factor of 4 above the value calculated for pure tungsten accumulation and we also find a strong rise of central Fe lines. The soft X-ray data show $m = 1$-mode activity without sawteeth, when ECRH is off. In the ECRH phase there are three minor sawtooth crashes at $t = 2.95$, 3.1 and 3.2 s, after the accumulation has disappeared.

Fig. 2 shows the result of impurity transport simulations for the above discharge #15524. Dashed lines give radial profiles for a time slice during the ECRH phase ($t = 3.5$–4.5 s) and solid lines are used for $t = 5.8$–6.0 s, which is at the end of the second pure NBI-heating phase. Neoclassical impurity transport coefficients were calculated numerically with NEOART [7–9], which can include the effect of impurity–impurity collisions for an arbitrary number of species. The transport simulation starts at $t = 1.5$ s with flat impurity concentrations and the impurity densities at the edge are kept constant during the simulation. In one case (light grey) only W was taken into account, while in the second case (dark grey) additional impurities were considered with 'typical' concentrations of 5% He, 1% C, 0.5% O, 0.02% Fe at the edge. n_e, T_e and T_i profiles were taken from measurements and n_i followed from the impurity ion distributions and quasi-neutrality. C, O, Fe and W are in the plateau regime with W at the Pfirsch-Schlüter limit, while D and He are in the banana regime. The anomalous diffusion coefficient was assumed to be equal for all impurity species and to decay from edge to center [10], where the central value was chosen to be $D_{an}(0) = 0.1$ m^2/s during ECRH and below neoclassical values during pure NBI heating. These choices are based on previous determinations of impurity transport coefficients between sawtooth crashes in sawtoothing H-mode discharges. Ne, Ar, Kr and Xe was investigated in purely NBI-heated discharges [1] and recent Si laser blow-off experiments revealed, that central ECRH with $P_{ECRH} = 0.8$ MW increases the central diffusion coefficient of Si to $D(0) = 0.1 \pm 0.05$ m^2/s, while discharges with pure NBI-heating or additional off-axis ECRH had $D(0) = 0.04 \pm 0.02$ m^2/s. The increased central diffusion coefficient with the additional central power flux from ECRH is interpreted to be a consequence of profile stiffness [11]. Analysis of the local heat diffusivities with ASTRA [12] yields an increase of central χ_i and χ_e. For $\rho = 0.3$ both values change from $\approx$0.2 m^2/s with ECRH off to $\approx$0.7 m^2/s with ECRH on. The calculated values of v/D are small in the ECRH phase, mainly due to the rather flat density profile and partly due to the increased D_{an}. In the pure NBI-phase, the density peaking increases, while D_{an} becomes small and v/D reaches large negative (inward pinch) values inside $\rho = 0.5$. In the case with inclusion of all impurities, the inward pinch is smaller and the v/D-profile is broader. The simulated W profile evolves the strongest peaking of all impurities as expected from Eq. (3). The calculated peaking of W is smaller than experimentally observed. This can be seen by comparing the calculated tungsten radiation profiles with the unfolded total radiation, which shows an even stronger peaking, even though there have to be large contributions from less peaked medium-Z metals to the total radiation. Similarly, the high central tungsten concentrations at the end of the discharge can only be simulated when setting the edge concentrations to 2–5 times the measured values depending on the inclusion of other impurities in the simulation. Perfect agreement can be achieved with a v/D profile that reaches a minimum value of -50 m^{-1}. Thus, the main features of the impurity flattening with ECRH and the strong peaking without ECRH are well described by the simulation and calculated v/D values agree with the measurement within a factor of 2. It should be mentioned, that also the evolution of the main ion density can be understood by a higher anomalous diffusion being connected to higher χ in the ECRH phase. The increase of D_{an} counteracts the neoclassical inward drift due to the Ware pinch [11]. Tungsten has a much higher collisionality and the Ware pinch, which is included in the simulations was found to yield a negligible contribution to the drift of W. For $t = 5.8$–6 s, the T_i gradient is increased and the related outwardly directed drift velocity is $\approx$50% above the value during the ECRH phase. Thus, the central radiation is still not large enough to change

the temperature screening and to trigger the instability described in [13].

2. ITB discharges with reversed shear at JET

The behaviour of carbon, neon and metallic impurities in JET-discharges with an ITB has been investigated using charge exchange recombination spectroscopy and emission profiles in the soft X-ray wavelength range [14,15]. The analysed ITB discharges had a current profile with strongly reversed shear at the start time of the main heating power phase [16]. The evolution of very high central soft X-ray emissions after the barrier formation was observed, which cannot be explained by low-Z impurities (Be, C and Ne) mainly emitting bremsstrahlung in the core. The strong emission must be due to line radiation of metallic elements and Ni is assumed to be the predominant metallic impurity. The radiation from low-Z elements is calculated taking the impurity densities of C and Ne (for discharges with Ne puffing) from CXRS into account, where the C emission is increased by 50% as an estimate for the contribution from other low-Z elements Be, N and F. Ni densities are calculated from the remaining difference to the total soft X-ray emission.

An example for the evolution of C, Ne and Ni densities in discharge #51976 [17] with a high performance ITB of 1 s duration gives Fig. 3. Before the formation of the strong barrier, at $t = 45.8$ s, T_i has an almost constant gradient length for the depicted radial range, and the impurity density profile is hollow or mildly peaked. A strong barrier in T_i, T_e and n_e forms at $t \approx 45.9$ s. At $t = 46.2$ s, the normalized T_i gradient is increased at a mid-plane radius of $R \approx 3.5$ m. The radius with increased normalized T_i gradient shifts towards larger radii for the following time slices due to an expansion of the barrier width and due to the increasing Shavranov shift. For the later times, the radial region of the T_i barrier location is depicted by a vertical light grey bar. Inside that region T_i becomes progressively flat. Here, n_e and the impurity densities develop the strongest gradient and the radial region with increased density gradients is given by a darker grey bar. The impurity peaking increases with the impurity charge Z and is weakest for C and very strong for Ni. At $t = 46.9$ s, the dominant Z_{eff} contribution is due to Ni and reaches a value of $\Delta Z_{eff} = 1.5$ for $Z_{eff} = 3.5$ causing a dilution of $\Delta n_e/n_e = 6\%$. Thus, the n_i profile has not much reduced peaking compared with n_e.

Neoclassical transport parameters were evaluated for #51976. In Fig. 4(a), the collision frequencies of Ni with D, C, Ne and Ni are shown for #51976 at $t = 46.6$ s. The collisions of Ni with C and Ne are as frequent as the collisions with D and had to be considered in the neoclassical calculation. The classical, Pfirsch-Schlüter and

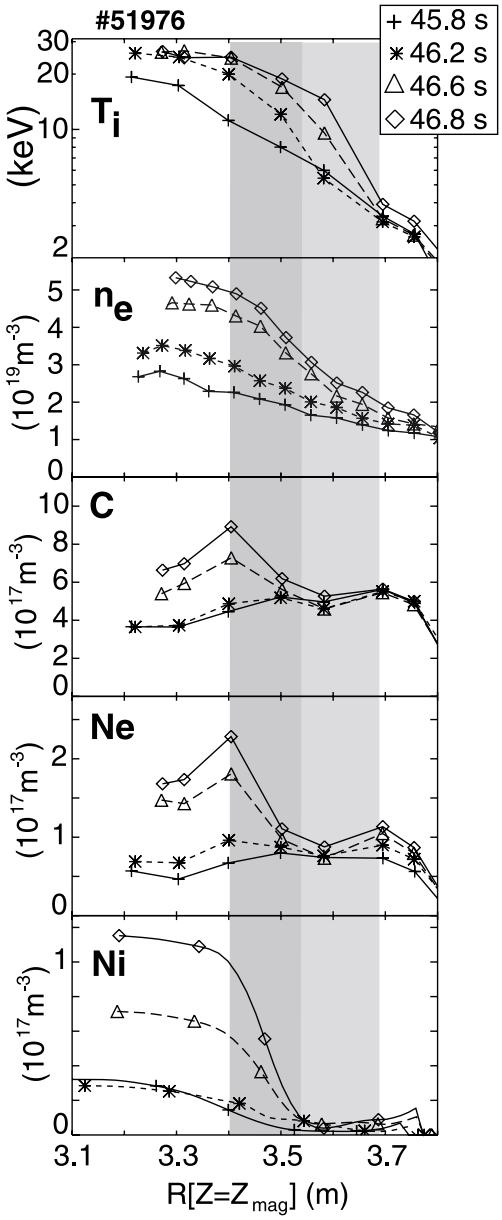

Fig. 3. Evolution of the radial profiles of T_i, n_e, n_C, n_{Ne} and n_{Ni} for the discharge #51976.

banana-plateau contribution was calculated by solving the coupled equations for the parallel velocities of a four component plasma (D, C, Ne, Ni) with NEOART using the fractional abundances of the different ion stages from the impurity transport code STRAHL. The required gradients of the densities and of T_i were taken from the experiment as shown in Fig. 3, where the deuterium density follows from n_e, the impurity densities and quasi-neutrality. Equal temperature of all ion species was assumed. In Fig. 4(b) the calculated radial

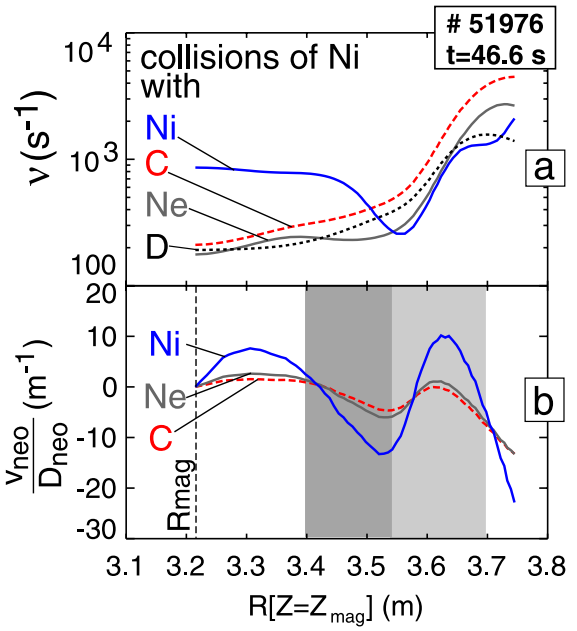

Fig. 4. Radial profile for the collision frequencies of Ni and the ratio v_{neo}/D_{neo} for C, Ne and Ni in discharge #51976 at $t = 46.6$ s.

profile of v_{neo}/D_{neo} is depicted for C, Ne and Ni. Close to the axis ($R \leqslant 3.35$ m) the poloidal field becomes very low, the orbits of trapped particles are very large and standard neoclassical theory may not be applied. In the region with weaker temperature gradient and pronounced electron peaking (dark grey bar in Figs. 4(b) and 3), the neoclassical transport is strongly convective with inwardly directed (negative) drift velocities. The absolute value of v_{neo}/D_{neo} rises with Z as experimentally observed. In the region with the strong temperature gradient (light grey bar in Figs. 4(b) and 3) the drift term is close to zero or becomes outwardly directed for the case of Ni. Thus the impurity behaviour can be understood in terms of neoclassical transport, where the drift velocities are governed by the ratio of the temperature to the density gradient. The evaluated values of v_{neo}, however, have a high uncertainty due to the uncertainty of all the gradients which enter into the calculation and the comparison is thus more qualitative.

In reversed shear discharges, which had long ITB phases of several seconds at reduced performance [18], strong accumulation of Ni was found in some cases, while C concentration profiles were almost flat. In such plasmas, a peaking of the n_e profile was observed. For the worst case, the accumulated Ni caused a maximum central $\Delta Z_{eff} = 5$ with a dilution due to Ni of $\Delta n_e/n_e = 20\%$ and central radiation losses approximately equal to the heating power density. However, there are also plasmas, which during the late phase of the discharge develop an ITB with weak n_e peaking which is accompanied by a complete recovery from an earlier Ni accumulation. Central T_i values are similar to the first type having only slightly reduced performance. MHD events, which lead to a sawtooth-like signature of T_e, correlate with a temporal decrease of the central Ni density during the accumulation. Further investigation is needed for these phenomena.

3. Conclusion

In improved H-mode scenarios at ASDEX Upgrade and ITB discharges with strongly reversed shear at JET, accumulation of metallic and high-Z impurities occurs in the central part of the plasma in cases with sufficiently strong peaking of the main ion density. This behaviour can be attributed to neoclassical inward convection, which is not counteracted by anomalous diffusion. In ASDEX Upgrade, central heating with ECRH increases the anomalous diffusion in the center leading to flatter main ion density profiles and a complete suppression of tungsten accumulation without sawteeth.

Acknowledgements

Part of this work was performed under the European Fusion Development Agreement (EFDA).

References

[1] R. Dux, A.G. Peeters, A. Gude, A. Kallenbach, R. Neu, et al., Nucl. Fusion 39 (1999) 1509.
[2] R. Neu, R. Dux, A. Geier, A. Kallenbach, R. Pugno, et al., Plasma Phys. Control. Fusion 44 (2002) 811.
[3] O. Gruber, R.C. Wolf, R. Dux, C. Fuchs, S. Günter, et al., Phys. Rev. Lett. 83 (1999).
[4] A.C.C. Sips, G.D. Conway, R. Dux, A. Herrmann, J. Hobirk, et al., Plasma Phys. Control. Fusion 44 (2002) A151.
[5] K. Asmussen, K.B. Fournier, J.M. Laming, R. Neu, J.F. Seely, et al., Nucl. Fusion 38 (1998) 967.
[6] R. Neu, K. Fournier, D. Bolshukhin, R. Dux, Phys. Scr. T92 (2001) 307.
[7] A.G. Peeters, Phys. Plasmas 7 (2000) 268.
[8] R. Dux, A.G. Peeters, Nucl. Fusion 40 (2000) 1721.
[9] S.P. Hirshman, D.J. Sigmar, Nucl. Fusion 21 (1981) 1079.
[10] ASDEX Upgrade Team, S. de Peña Hempel, R. Dux, A. Kallenbach, H. Meister, in: M. Schittenhelm, R. Bartiromo, F. Wagner (Eds.), Europhysics Conference Abstracts, (Proc. of the 24th EPS Conference on Controlled Fusion and Plasma Physics, Berchtesgaden, 1997), vol. 21A, part IV, EPS, Petit-Lancy, 1997, p. 1401.
[11] J. Stober, C. Fuchs, M. Kaufmann, B. Kurzan, F. Meo, et al., Nucl. Fusion 41 (2001) 1535.

[12] G. Pereverzev, P.N. Yushmanov, 'ASTRA Automated System for Transport Analysis in a Tokamak', IPP-5/98, Max-Planck-Institut für Plasmaphysik, Garching, Germany, 2002.
[13] M.Z. Tokar, J. Rapp, G. Bertschinger, L. Könen, A. Krämer-Flecken, et al., Nucl. Fusion 37 (1997) 1691.
[14] R. Dux, C. Giroud, C. Ingesson, K.-D. Zastrow, the Contributors to the EFDA-JET Workprogramme, in: 28th Conference on Controlled Fusion and Plasma Physics, Madeira, P2.007, EPS, 2001.
[15] C. Giroud, K.-D. Zastrow, P. Andrew, R. Dux, P. Morgan, et al., in: 28th Conference on Controlled Fusion and Plasma Physics, Madeira, P2.018, EPS, 2001.
[16] N.C. Hawkes, B.C. Stratton, T. Tala, et al., Phys. Rev. Lett. 87 (2001) 115001.
[17] C.D. Challis, X. Litaudon, G. Tresset, Y.F. Baranov, A. Bècoulet, et al., Plasma Phys. Control. Fusion 44 (2002) 1031.
[18] F. Crisanti, X. Litaudan, et al., Phys. Rev. Lett. 88 (2002) 145004.